Computers & Fluids 42 (2011) 54–61

Contents lists available at ScienceDirect

Computers & Fluids

journal homepage: www.elsevier.com/locate/compfluid

# Numerical solution of a phase field model for incompressible two-phase flows based on artificial compressibility

Abdullah Shah [a,*], Li Yuan [b]

[a] Department of Mathematics, COMSATS Institute of Information Technology, Park Road, Islamabad 44000, Pakistan
[b] LSEC and Institute of Computational Mathematics and Scientific/Engineering Computing, Academy of Mathematics & Systems Science, Chinese Academy of Sciences, Beijing 100190, PR China

ARTICLE INFO

*Article history:*
Received 2 April 2010
Received in revised form 12 October 2010
Accepted 31 October 2010
Available online 10 November 2010

*Keywords:*
Two-phase flow
Phase field model
Incompressible Navier–Stokes equations
Artificial compressibility
WENO scheme

ABSTRACT

We present an artificial compressibility based numerical method for a phase field model for simulating two-phase incompressible viscous flows. The phase model was proposed by Liu and Shen [Physica D. 179 (2003) 211–228], in which the interface between two fluids is represented by a thin transition region of fluid mixture that stores certain amount of mixing energy. The model consists of the Navier–Stokes equations coupled with the Allen–Cahn equation (phase field equation) through an extra stress term and a transport term. The extra stress in the momentum equations represents the phase-induced capillary effect for the mixture due to the surface tension. The coupled equations are cast into a conservative form suitable for implementation with the artificial compressibility method. The resulting hyperbolic system of equations are then discretized with weighted essentially non-oscillatory (WENO) finite difference scheme. The dual-time stepping technique is applied for obtaining time accuracy at each physical time step, and the approximate factorization algorithm is used to solve the discretized equations. The effectiveness of the numerical method is demonstrated in several two-phase flow problems with topological changes. Numerical results show the present method can be used to simulate incompressible two-phase flows with small interfacial width parameters and topological changes.



## 1. Introduction

The nature of the interface between two fluids has been the subject of extensive investigation in many scientific and engineering applications for two centuries. The initial investigations dated back to Young, Laplace and Gauss, who considered the interface between two fluids as a zero thickness (sharp) surface endowed with some physical properties such as surface tension [1]. Latter, Poisson, Maxwell and Gibbs recognized that the interface in fact represented a rapid but smooth transition layer, where the physical quantities smoothly changed between two different bulk values. Such a diffuse-interface idea gained further development later, and in the works of Rayleigh [2], van der Waals [3], among others, it was shaped into gradient theories for the interface based on thermodynamical principles.

A contemporary representative theory for the diffuse-interface notion that had root in Rayleigh and van der Waals ideas is the phase field (PF) model. In a PF model, the sharp fluid interface is replaced by a thin but nonzero thickness transition layer, where the interfacial force is smoothly distributed as a capillary stress tensor. Within this transition layer, fluids are mixed and have to store certain amount of mixing energy. The mixture can be treated as a special type of non-Newtonian fluid. The final rheology property reflects the competition between the kinetic energy and the elastic mixing energy [4]. The energetics of the thermodynamic system described in terms of either the grand potential or the total energy function can be modified to incorporate the effects of the evolving phase field, thus gaining similarity with the energy contributions from the surface excess quantities introduced in the Gibbs formulation of surface thermodynamics [5]. When the capillary width approaches zero, the PF model reduces properly to the classical sharp interface model.

From the methodology point of view, the PF model can be viewed as a physically motivated indicator function method (typical indicator functions include level-set, volume of fraction, etc.). Rather than choosing an artificial smoothing function for the interface, which contaminates the results in non-trivial ways if the radius of interfacial curvature approaches that of the interfacial thickness [6], the PF model describes the interface by physically profound mixing energy. The main attraction of the phase field model is its capability to easily incorporate the complex rheology of microstructured fluids with smooth transition of physical quantities. Thus, the PF model provides a sound alternative for problems

* Corresponding author. Tel.: +92 333 9436650; fax: +92 51 4442805.
*E-mail addresses:* scholar.cm@gmail.com (A. Shah), lyuan@lsec.cc.ac.cn (L. Yuan).

0045-7930/$ - see front matter © 2010 Elsevier Ltd. All rights reserved.
doi:10.1016/j.compfluid.2010.10.021

with topologically complex interfaces and problems, where the interface thickness is comparable to the length scale of the phenomena being involved. In recent years, the PF model is an increasingly popular choice for modeling many kinds of application problems ranging from free surface flows to critical phenomena (see reference [7] for a detailed review, and [8] for advantages and challenges and references there in).

There are many varieties of PF models. Recently, Liu and Shen proposed a new formulation of PF model [4]. Their model was based on an energetic variational formulation, and was shown to be suitable for a wide range of applications and numerical methods [9–16]. In their formulation, a mixing energy is defined based on the phase variable $\phi$, through which a convection–diffusion equation governing the evolution of the interfacial profile is derived. The dynamic of $\phi$ can be driven by either Allen–Cahn [17] or Cahn–Hilliard [18] types of gradient flows, depending on the choice of dissipative mechanism. The elastic (mixing) energy is responsible for the appearance of the induced elastic stress in the momentum equations. The variable $\phi$ assumes distinct constant values in each bulk phase and undergoes rapid but smooth variation in the interfacial region. When thickness of the interface approaches zero, this PF model is proven convergent to the sharp interface level-set formulation [19–21].

In this work, numerical solution to the PF model of Liu and Shen for incompressible two-fluid mixture [4] was realized by using the artificial compressibility method [22]. The numerical simulation of small thickness cases poses difficulty to numerical methods. Since numerical implementation of the Allen–Cahn type of dynamics is simpler than the Cahn–Hilliard type which involves the fourth-order differential operator, we choose the former formalism. It is well-known that Allen–Cahn type of dynamics induces volume dissipation, yet this can be controlled by introducing a Lagrange multiplier [4,14]. Thus, the present PF model consists of the incompressible Navier–Stokes equations with two additions: the Allen–Cahn type equation for the phase field variable $\phi$, and an extra stress tensor in the momentum equations which represents capillary effect for the mixture due to the surface tension.

In previous numerical implementation of this PF model, projection methods were often used [16,23,24]. These methods are generally very accurate for divergence-free constraint and efficient for time-dependent problems. However, their extension to general curvilinear coordinates is rather involved, and the stiffness of very thin transitional layer may incur exceedingly small time step. On the other hand, numerical discretization of the artificial compressibility method will be simpler in general curvilinear coordinates and easier to solve than an elliptic system, as a conservative form of pseudo-time hyperbolic system is formulated and a time marching scheme can be used. For such conservative laws, many high-order high-resolution schemes like WENO scheme [25,26] can be used to better capture the thin diffusive layer and various implicit schemes can be utilized to relieve time step limitation, especially for cases, where the width parameter of the diffusive layer is set to small value. Of course, the artificial compressibility method has a major disadvantage that the incompressibility constraint is satisfied only when the hyperbolic system is marched in pseudo-time to a converged state, which is generally inefficient for time-dependent problems. Nevertheless, it may not be a big problem if the dual-time stepping technique [27,28] is used together with an efficient sub-iteration method.

This paper is organized as follows. In Section 2, the governing equations for the mixture of two incompressible fluids are provided with relevant details. In Section 3, formulations based on the artificial compressibility method are rewritten in conservative form. Section 4 explains the spatial discretization. Time discretization and numerical implementation are given in Section 5. Numerical tests in several two-dimensional problems on the mixture of two incompressible fluids are given in Section 6. Section 7 concludes this paper.

## 2. Phase field model for mixture of two incompressible fluids

Let $\Omega$ be a two-dimensional physical domain that is filled with two incompressible viscous fluids separated by a thin transitional layer. The phase field function $\phi(\mathbf{x},t)$ assumes distinct constant values in each bulk phase and undergoes rapid but smooth variation in the interfacial region. It is used to identify the two fluids and the interface at any time $t$ by the following relation

$$\begin{cases} \mathbf{x} : \phi(\mathbf{x},t) = -1 & \text{fluid 1}, \\ \mathbf{x} : \phi(\mathbf{x},t) = 0 & \text{interface}, \\ \mathbf{x} : \phi(\mathbf{x},t) = 1 & \text{fluid 2}. \end{cases}$$

We have adopted the PF model [4] which uses the familiar Ginzburg–Landau form of elastic (mixing) energy for the interaction between the two fluids

$$W(\phi,\nabla\phi) = \int_\Omega \left(\frac{1}{2}|\nabla\phi|^2 + F(\phi)\right) dx, \tag{2.1}$$

where

$$F(\phi) = \frac{1}{4\eta^2}\left(|\phi|^2 - 1\right)^2, \tag{2.2}$$

is a usual double-well potential of the bulk energy with $\eta$ being the interfacial width (width of the mixing layer).

The evolution of $\phi$ is governed by either of the following equations:

$$\phi_t + \mathbf{u}\cdot\nabla\phi = \begin{cases} -\gamma\frac{\delta W}{\delta\phi} = \gamma(\Delta\phi - f(\phi)) & \text{Allen—Cahn equation}, \\ \nabla\cdot\left(\gamma\nabla\frac{\delta W}{\delta\phi}\right) = -\gamma\Delta(\Delta\phi - f(\phi)) & \text{Cahn—Hilliard equation}. \end{cases} \tag{2.3}$$

Here $\delta W/\delta\phi$ represents the variation of the energy $W$ with respect to $\phi$, $f(\phi)$ is a polynomial of $\phi$ such that $f(\phi) = F'(\phi) = \frac{\phi(\phi^2-1)}{\eta^2}$, and constant $\gamma$ represents the elastic relaxation time. The Allen–Cahn equation differs from the Cahn–Hilliard equation in that the later satisfies the volume fraction conservation constraint. However, numerical solution of the Cahn–Hilliard equation is more difficult than the Allen–Cahn equation because of the more complicated fourth-order Laplacian operator and the nonlinear terms. In this work, we choose the modified Allen–Cahn equation[14] which gives simplification in formulation and satisfies the volume fraction conservation constraint. The momentum equation for the fluid flow takes the form

$$\rho[\mathbf{u}_t + (\mathbf{u}\cdot\nabla)\mathbf{u}] = -\nabla p + \nabla\cdot\sigma, \tag{2.4}$$

where $\rho$ is the density of mixture, $p$ is the pressure and $\sigma$ is the stress tensor that includes the viscous tensor and the induced elastic stress tensor (due to mixing of different fluids) and is given by

$$\sigma = \mu\left[\nabla\mathbf{u} + (\nabla\mathbf{u})^T\right] - \lambda\nabla\phi\otimes\nabla\phi, \tag{2.5}$$

where $\mu$ is the fluid viscosity of mixture, $\lambda$ is the surface tension coefficient and $(\nabla\phi\otimes\nabla\phi)_{ij} = \nabla_i\phi\nabla_j\phi$ is the usual tensor product. By using the identity

$$\nabla\cdot(\nabla\phi\otimes\nabla\phi) = \Delta\phi\nabla\phi + \nabla\left(\frac{1}{2}|\nabla\phi|^2\right), \tag{2.6}$$

the momentum equation is further simplified by redefining the pressure term: $p = p + \frac{1}{2}\lambda|\nabla\phi|^2$.

In this work, we restrict to a specific type of mixture of two incompressible fluids with same density ($\rho = 1$ for simplicity)

and same viscosity constants ($\mu_1 = \mu_2 = \mu$) [4,14]. So, we have the following system of governing equations:

$$\nabla \cdot \mathbf{u} = 0, \tag{2.7a}$$
$$\mathbf{u}_t + \nabla \cdot (\mathbf{u}\mathbf{u}) - \mu\Delta\mathbf{u} + \nabla p = -\lambda\Delta\phi\nabla\phi, \tag{2.7b}$$
$$\phi_t + \nabla \cdot (\mathbf{u}\phi) - \gamma\Delta\phi = \gamma(-f(\phi) + \xi(t)), \tag{2.7c}$$
$$\frac{d}{dt}\int_\Omega \phi dx = 0, \tag{2.7d}$$

where the momentum equation and the Allen–Cahn equation are written in divergence form by virtue of (2.7a). The coupled nonlinear system (2.7) will be subject to the initial conditions

$$\mathbf{u}|_{t=0} = \mathbf{u}_0, \qquad \phi|_{t=0} = \phi_0,$$

and appropriate boundary conditions. The role of the Lagrange multiplier $\xi(t)$ in the Allen–Cahn equation is to change the asymptotic constant values (±1) of the phase function $\phi$ so as to conserve the volume fraction (2.7d). In practice, the $\xi(t)$ in Eq. (2.7c) is modified as $\xi(t)(1-\phi^2)$ because this will keep the maximum principle for $\phi$ as noted in [14]. The new $\xi(t)$ can be calculated by using the following formula

$$\xi(t) = \int_\Omega f(\phi)dx \Big/ \int_\Omega (1-\phi^2)dx.$$

## 3. Artificial compressibility formulation

By adding the artificial compressibility terms for dual-time stepping technique, the system (2.7a)–(2.7c) in two space dimensions can be rewritten as follows:

$$p_\tau + \beta(u_x + v_y) = 0, \tag{3.1a}$$
$$u_\tau + u_t + (u^2+p)_x + (uv)_y - \mu(u_{xx}+u_{yy}) = -\lambda\phi_x(\phi_{xx}+\phi_{yy}), \tag{3.1b}$$
$$v_\tau + v_t + (uv)_x + (v^2+p)_y - \mu(v_{xx}+v_{yy}) = -\lambda\phi_y(\phi_{xx}+\phi_{yy}), \tag{3.1c}$$
$$\phi_\tau + \phi_t + (u\phi)_x + (v\phi)_y - \gamma(\phi_{xx}+\phi_{yy}) = \gamma(1-\phi^2)\left(\frac{\phi}{\eta^2} + \xi(t)\right). \tag{3.1d}$$

Write the above equations in conservative form with source term:

$$\mathbf{Q}_\tau + \mathbf{I}_m\mathbf{Q}_t + (\mathbf{E}-\mathbf{E}_v)_x + (\mathbf{F}-\mathbf{F}_v)_y = \mathbf{S}_{\text{int}}, \tag{3.2}$$

with

$$\mathbf{Q} = \begin{bmatrix} p \\ u \\ v \\ \phi \end{bmatrix}, \quad \mathbf{E} = \begin{bmatrix} \beta u \\ u^2+p \\ uv \\ u\phi \end{bmatrix}, \quad \mathbf{F} = \begin{bmatrix} \beta v \\ uv \\ v^2+p \\ v\phi \end{bmatrix}, \quad \mathbf{I}_m = \begin{bmatrix} 0 & 0 & 0 & 0 \\ 0 & 1 & 0 & 0 \\ 0 & 0 & 1 & 0 \\ 0 & 0 & 0 & 1 \end{bmatrix},$$

and

$$\mathbf{E}_v = \begin{bmatrix} 0 \\ \mu u_x \\ \mu v_x \\ \gamma\phi_x \end{bmatrix}, \quad \mathbf{F}_v = \begin{bmatrix} 0 \\ \mu u_y \\ \mu v_y \\ \gamma\phi_y \end{bmatrix}, \quad \mathbf{S}_{\text{int}} = \begin{bmatrix} 0 \\ -\lambda\phi_x(\phi_{xx}+\phi_{yy}) \\ -\lambda\phi_y(\phi_{xx}+\phi_{yy}) \\ \gamma(1-\phi^2)(\phi/\eta^2 + \xi(t)) \end{bmatrix}.$$

Here $\mathbf{Q}$ is the solution vector, $u$ and $v$ are Cartesian velocity components, $p$ is the redefined pressure, $\phi$ represents the phase variable of the species, $\mu$ is the viscosity constant, $\beta$ is the artificial compressibility factor, $\tau$ is the pseudo-time and $t$ is the physical time. The matrix $\mathbf{I}_m$ is a modified identity matrix. $\mathbf{S}_{\text{int}}$ is the contribution from the capillary effect and the nonlinear term in the phase field equation. Subscripts $\tau$, $t$, $x$,$y$ represent partial derivatives. Because of the addition of the artificial compressibility terms, the equations become hyperbolic with respect to the pseudo-time, with Jacobian matrices $\mathbf{A}$ and $\mathbf{B}$ of the inviscid flux vectors $\mathbf{E}$ and $\mathbf{F}$ respectively and are given by

$$\mathbf{A} = \frac{\partial\mathbf{E}}{\partial\mathbf{Q}} = \begin{bmatrix} 0 & \beta & 0 & 0 \\ 1 & 2u & 0 & 0 \\ 0 & v & u & 0 \\ 0 & \phi & 0 & u \end{bmatrix}, \quad \mathbf{B} = \frac{\partial\mathbf{F}}{\partial\mathbf{Q}} = \begin{bmatrix} 0 & 0 & \beta & 0 \\ 0 & v & u & 0 \\ 1 & 0 & 2v & 0 \\ 0 & 0 & \phi & v \end{bmatrix}.$$

The viscous Jacobian matrices $\mathbf{A}_v$ and $\mathbf{B}_v$ of the viscous flux vectors $\mathbf{E}_v$ and $\mathbf{F}_v$ respectively, which will be utilized in the approximate factorization scheme are

$$\mathbf{A}_v = \frac{\partial\mathbf{E}_v}{\partial\mathbf{Q}} = \text{diag}(0,\mu,\mu,\gamma)\partial_x, \quad \text{and} \quad \mathbf{B}_v = \frac{\partial\mathbf{F}_v}{\partial\mathbf{Q}} = \text{diag}(0,\mu,\mu,\gamma)\partial_y. \tag{3.3}$$

It is possible to diagonalize $\mathbf{A}$ and $\mathbf{B}$ as

$$\mathbf{A} = \mathbf{X}\Lambda_A\mathbf{X}^{-1}, \quad \mathbf{B} = \mathbf{Y}\Lambda_B\mathbf{Y}^{-1}, \tag{3.4}$$

where diagonal matrices $\Lambda_A$ and $\Lambda_B$ contain the eigenvalues of matrices $\mathbf{A}$ and $\mathbf{B}$ respectively:

$$\text{diag}\,\Lambda_A = \{u, u+c_1, u-c_1, u\}, \ \text{diag}\,\Lambda_B = \{v, v+c_2, v-c_2, v\}, \tag{3.5}$$

with $c_1 = \sqrt{u^2+\beta}$ and $c_2 = \sqrt{v^2+\beta}$ being the pseudo-speeds of sound. The matrices $\mathbf{X}$ and $\mathbf{Y}$ are the right eigenvectors matrices, while $\mathbf{X}^{-1}$ and $\mathbf{Y}^{-1}$ are their inverses respectively. These matrices are given by

$$\mathbf{X} = \begin{bmatrix} 0 & c_1(c_1-u) & c_1(c_1+u) & 0 \\ 0 & c_1 & -c_1 & 0 \\ 1 & v & v & 0 \\ 0 & \phi & \phi & 1 \end{bmatrix},$$

$$\mathbf{X}^{-1} = \frac{1}{(c_1)^2}\begin{bmatrix} -v & -uv & c_1^2 & 0 \\ \frac{1}{2} & \frac{1}{2}(c_1+u) & 0 & 0 \\ \frac{1}{2} & -\frac{1}{2}(c_1-u) & 0 & 0 \\ -\phi & -u\phi & 0 & c_1^2 \end{bmatrix}$$

and

$$\mathbf{Y} = \begin{bmatrix} 0 & c_2(c_2-v) & c_2(c_2+v) & 0 \\ 1 & u & u & 0 \\ 0 & c_2 & -c_2 & 0 \\ 0 & \phi & \phi & 1 \end{bmatrix},$$

$$\mathbf{Y}^{-1} = \frac{1}{(c_2)^2}\begin{bmatrix} -u & c_2^2 & -uv & 0 \\ \frac{1}{2} & 0 & \frac{1}{2}(c_2+v) & 0 \\ \frac{1}{2} & 0 & -\frac{1}{2}(c_2-v) & 0 \\ -\phi & 0 & -v\phi & c_2^2 \end{bmatrix}$$

## 4. Spatial discretization

To overcome the difficulty caused by the stiffness of sharp interface situations (the interface width $\eta \to 0$), we will use the weighted essentially non-oscillatory (WENO) scheme [25,26] for discretizing the convective terms. WENO scheme is a high order and high-resolution shock-capturing scheme widely used for solving the compressible Euler equations. Conventional second-order central schemes will be used for the viscous terms and the surface tension terms. We use a finite difference version of WENO scheme similar to that implemented for the artificial compressibility method in [26] but with different split fluxes. Uniform Cartesian meshes are used in this work. Let the mesh size in the $x$-direction be $\Delta x$ and the grid point be $x_j = j\Delta x$. Various quantities at $x_j$ will be

identified by the subscript $j$. The WENO scheme which approximates $\mathbf{E}_x$ at $x_j$ will take the conservative form

$$\mathbf{E}_x = \frac{\widetilde{\mathbf{E}}_{j+1/2} - \widetilde{\mathbf{E}}_{j-1/2}}{\Delta x}, \tag{4.1}$$

where $\widetilde{\mathbf{E}}_{j+1/2}$ and $\widetilde{\mathbf{E}}_{j-1/2}$ are the numerical fluxes. We implement WENO scheme in the characteristic way. Designate $f_k^{s+}$ and $f_k^{s-}$ respectively the local Lax–Friedriches fluxes in the $s$th characteristic field:

$$f_k^{s\pm} = \frac{f_k^s \pm \alpha_s W_k^s}{2}, \qquad k = j-2, \cdots, j+3, \tag{4.2}$$

with

$$f_k^s = \mathbf{L}_{j+\frac{1}{2}}^s \cdot \mathbf{E}_k, \quad W_k^s = \mathbf{L}_{j+\frac{1}{2}}^s \cdot \mathbf{Q}_k,$$

where $\mathbf{L}_{j+\frac{1}{2}}^s$ is the $s$th left eigenvector, evaluated for arithmetic average state between $j$ and $j+1$, and $\alpha_s$ is the maximum magnitude of the $s$th eigenvalue of Jacobian matrix $\mathbf{A}_{k+\frac{1}{2}}$ over the range of $(k = j-2, \ldots, j+2)$ for the local flux splitting. Following contents of this section are identical to that given in Ref. [26]. First, we describe the approximation of the numerical fluxes in the $s$th characteristic field. The WENO numerical flux for the positive part $\tilde{f}_{j+\frac{1}{2}}^{s+}$ is

$$\begin{aligned}\tilde{f}_{j+\frac{1}{2}}^{s+} &= \omega_0^+\left(\frac{2}{6}f_{j-2}^{s+} - \frac{7}{6}f_{j-1}^{s+} + \frac{11}{6}f_j^{s+}\right) + \omega_1^+\left(-\frac{1}{6}f_{j-1}^{s+} + \frac{5}{6}f_j^{s+} + \frac{2}{6}f_{j+1}^{s+}\right)\\ &\quad + \omega_2^+\left(\frac{2}{6}f_j^{s+} + \frac{5}{6}f_{j+1}^{s+} - \frac{1}{6}f_{j+2}^{s+}\right),\end{aligned} \tag{4.3}$$

where

$$\omega_k^+ = \frac{\alpha_k^+}{\alpha_0^+ + \alpha_1^+ + \alpha_2^+}, \quad k = 0, 1, 2$$

$$\alpha_0^+ = \frac{1}{10}(\epsilon + \mathrm{IS}_0^+)^{-2}, \quad \alpha_1^+ = \frac{6}{10}(\epsilon + \mathrm{IS}_1^+)^{-2},$$
$$\alpha_2^+ = \frac{3}{10}(\epsilon + \mathrm{IS}_2^+)^{-2}, \quad \epsilon = 10^{-6}$$

and

$$\begin{aligned}\mathrm{IS}_0^+ &= \frac{13}{12}\left(f_{j-2}^{s+} - 2f_{j-1}^{s+} + f_j^{s+}\right)^2 + \frac{1}{4}\left(f_{j-2}^{s+} - 4f_{j-1}^{s+} + 3f_j^{s+}\right)^2\\ \mathrm{IS}_1^+ &= \frac{13}{12}\left(f_{j-1}^{s+} - 2f_j^{s+} + f_{j+1}^{s+}\right)^2 + \frac{1}{4}\left(f_{j-1}^{s+} - f_{j+1}^{s+}\right)^2\\ \mathrm{IS}_2^+ &= \frac{13}{12}\left(f_j^{s+} - 2f_{j+1}^{s+} + f_{j+2}^{s+}\right)^2 + \frac{1}{4}\left(3f_j^{s+} - 4f_{j+1}^{s+} + f_{j+2}^{s+}\right)^2.\end{aligned}$$

Similarly, the WENO numerical flux for the negative part $\tilde{f}_{j+\frac{1}{2}}^{s-}$ is

$$\begin{aligned}\tilde{f}_{j+\frac{1}{2}}^{s-} &= \omega_0^-\left(-\frac{1}{6}f_{j-1}^{s-} + \frac{5}{6}f_j^{s-} + \frac{2}{6}f_{j+1}^{s-}\right) + \omega_1^-\left(\frac{2}{6}f_j^{s-} + \frac{5}{6}f_{j+1}^{s-} - \frac{1}{6}f_{j+2}^{s-}\right)\\ &\quad + \omega_2^-\left(\frac{11}{6}f_{j+1}^{s-} - \frac{7}{6}f_{j+2}^{s-} + \frac{2}{6}s_{j+3}^{s-}\right),\end{aligned} \tag{4.4}$$

where

$$\omega_k^- = \frac{\alpha_k^-}{\alpha_0^- + \alpha_1^- + \alpha_2^-}, \qquad k = 0, 1, 2$$

$$\alpha_0^- = \frac{3}{10}(\epsilon + \mathrm{IS}_0^-)^{-2}, \quad \alpha_1^- = \frac{6}{10}(\epsilon + \mathrm{IS}_1^-)^{-2},$$
$$\alpha_2^- = \frac{1}{10}(\epsilon + \mathrm{IS}_2^-)^{-2}, \quad \epsilon = 10^{-6}$$

and

$$\begin{aligned}\mathrm{IS}_0^- &= \frac{13}{12}\left(f_{j-1}^{s-} - 2f_j^{s-} + f_{j+1}^{s-}\right)^2 + \frac{1}{4}\left(f_{j-1}^{s-} - 4f_j^{s-} + 3f_{j+1}^{s-}\right)^2\\ \mathrm{IS}_1^- &= \frac{13}{12}\left(f_j^{s-} - 2f_{j+1}^{s-} + f_{j+2}^{s-}\right)^2 + \frac{1}{4}\left(f_j^{s-} - f_{j+2}^{s-}\right)^2\\ \mathrm{IS}_2^- &= \frac{13}{12}\left(f_{j+1}^{s-} - 2f_{j+2}^{s-} + f_{j+3}^{s-}\right)^2 + \frac{1}{4}\left(3f_{j+1}^{s-} - 4f_{j+2}^{s-} + f_{j+3}^{s-}\right)^2.\end{aligned}$$

Next, we convert the numerical flux back to the physical space. Denote $\mathbf{R}_{j+\frac{1}{2}}^s$ (column vector) the $s$th right eigenvector of Jacobian $\mathbf{A}_{j+\frac{1}{2}}$. The numerical fluxes obtained in each characteristic field can be projected back to the physical space by

$$\widetilde{\mathbf{E}}_{j+\frac{1}{2}} = \sum_{s=1}^{4} \tilde{f}_{j+\frac{1}{2}}^s \mathbf{R}_{j+\frac{1}{2}}^s = \sum_{s=1}^{4}\left(\tilde{f}_{j+\frac{1}{2}}^{s+} + \tilde{f}_{j+\frac{1}{2}}^{s-}\right)\mathbf{R}_{j+\frac{1}{2}}^s. \tag{4.5}$$

Other directions can be treated similarly.

## 5. Implicit approximate factorization scheme

The approximate factorization (AF) method [29] is an extension of the alternating direction implicit (ADI) method to the system of the Navier–Stokes equations. Applying backward difference to the pseudo-time derivative and three point, second-order backward difference scheme to the physical time derivative in Eq. (3.2), we obtain

$$\begin{aligned}&\frac{\Delta\mathbf{Q}^{n+1,m}}{\Delta\tau} + \mathbf{I}_m\frac{1.5\mathbf{Q}^{n+1,m+1} - 2\mathbf{Q}^n + 0.5\mathbf{Q}^{n-1}}{\Delta t}\\ &\quad + \left[\frac{\partial(\mathbf{E} - \mathbf{E}_v)}{\partial x} + \frac{\partial(\mathbf{F} - \mathbf{F}_v)}{\partial y}\right]^{n+1,m+1} = \mathbf{S}_{\mathrm{int}}^{n+1,m},\end{aligned} \tag{5.1}$$

where $\Delta\mathbf{Q}^{n+1,m} = \mathbf{Q}^{n+1,m+1} - \mathbf{Q}^{n+1,m}$, the superscript $n$ is the physical time level, and $m$ is the pseudo-time level (the number of sub-iterations). $\Delta\tau$ is the pseudo-time step size which is determined based on the CFL number and $\Delta t$ is the physical time step size. In this work, we treat $\mathbf{S}_{\mathrm{int}}$ explicitly. The equations are iterated in pseudo-time so that $\mathbf{Q}^{n+1,m+1}$ approaches the physical $\mathbf{Q}^{n+1}$ when the iteration is converged. The residual terms at $m+1$ pseudo-time level are linearized with respect to the previous level $m$ by using Taylor's expansion, e.g.

$$\mathbf{E}^{m+1} \approx \mathbf{E}(\mathbf{Q}^m) + \left(\frac{\partial\mathbf{E}}{\partial\mathbf{Q}}\right)^m(\mathbf{Q}^{m+1} - \mathbf{Q}^m) = \mathbf{E}^m + \mathbf{A}^m\Delta\mathbf{Q}^m. \tag{5.2}$$

From now on, the superscript $n+1$ is omitted for brevity. One can obtain the unfactored implicit delta form as

$$\begin{aligned}&\left[\mathbf{I} + 1.5\frac{\Delta\tau}{\Delta t}\mathbf{I}_m + \Delta\tau\left(\frac{\partial(\mathbf{A} - \mathbf{A}_v)}{\partial x} + \frac{\partial(\mathbf{B} - \mathbf{B}_v)}{\partial y}\right)\right]^m\Delta\mathbf{Q}^m\\ &\quad = -\Delta\tau\left(\frac{\partial(\mathbf{E} - \mathbf{E}_v)}{\partial x} + \frac{\partial(\mathbf{F} - \mathbf{F}_v)}{\partial y} - \mathbf{S}_{\mathrm{int}}\right)^m - \frac{\Delta\tau}{\Delta t}\mathbf{I}_m(1.5\mathbf{Q}^m - 2\mathbf{Q}^n\\ &\qquad + 0.5\mathbf{Q}^{n-1}) = \mathbf{R}^m.\end{aligned} \tag{5.3}$$

The terms $\mathbf{A}_v$ and $\mathbf{B}_v$ are the viscous Jacobian matrices given in Eq. (3.3). The Beam–Warming approximate factorization scheme [29] can be symbolically written as

$$\pounds\cdot\Delta\mathbf{Q}^m \approx \pounds_x\pounds_y\cdot\Delta\mathbf{Q}^m = \mathbf{R}^m. \tag{5.4}$$

To obtain block tri-diagonal equations, convective terms in LHS of Eq. (5.3) are discretized by first-order upwind difference and viscous terms by second-order central difference, e.g.

$$\delta_x^+ f_i = \frac{f_{i+1} - f_i}{\Delta x}, \quad \delta_x^- f_i = \frac{f_i - f_{i-1}}{\Delta x}, \text{ and } \quad \delta_x^2 f_i = \frac{(f_{i+1} - 2f_i + f_{i-1})}{\Delta x^2}.$$

Remember that WENO scheme is still used for the convective terms and central difference for the viscous and capillary terms in RHS. Thus, Eq. (5.3) becomes the following form

$$\left[\mathbf{I}+1.5\frac{\Delta\tau}{\Delta t}\mathbf{I}_m+\Delta\tau\left(\delta_x^-\mathbf{A}^+ +\delta_x^+\mathbf{A}^- -\delta_x\mathbf{A}_v\right)+\Delta\tau\left(\delta_y^-\mathbf{B}^+ +\delta_y^+\mathbf{B}^- -\delta_y\mathbf{B}_v\right)\right]^m \times\Delta\mathbf{Q}^m=\mathbf{R}^m. \tag{5.5}$$

In order to make use of the diagonal algorithm which saves computational cost [30,31], we change $\mathbf{I}_m$ to $\mathbf{I}$ and diag$(0,\mu,\mu,\gamma)$ to max$(\mu,\gamma)\mathbf{I}$ in the LHS of Eq. (5.5), which alters convergence but not accuracy. Denote $(1+1.5\frac{\Delta\tau}{\Delta t})\mathbf{I}=\mathbf{H}$, $\mu_m=\max(\mu,\gamma)$, then the equation becomes

$$\left[\mathbf{H}+\Delta\tau\left(\delta_x^-\mathbf{X}\mathbf{\Lambda}_A^+\mathbf{X}^{-1}+\delta_x^+\mathbf{X}\mathbf{\Lambda}_A^-\mathbf{X}^{-1}-\mu_m\mathbf{I}\delta_x^2\right) +\Delta\tau\left(\delta_y^-\mathbf{Y}\mathbf{\Lambda}_B^+\mathbf{Y}^{-1}+\delta_y^+\mathbf{Y}\mathbf{\Lambda}_B^-\mathbf{Y}^{-1}-\mu_m\mathbf{I}\delta_y^2\right)\right]^m\Delta\mathbf{Q}^m=\mathbf{R}^m. \tag{5.6}$$

As usual, by adding cross-derivative terms to LHS of (5.6), which is the same order of $\Delta\tau^3$ as the truncated terms of original equations, we can obtain the AF scheme in the following form

$$\left[\mathbf{H}+\Delta\tau\left(\delta_x^-\mathbf{X}\mathbf{\Lambda}_A^+\mathbf{X}^{-1}+\delta_x^+\mathbf{X}\mathbf{\Lambda}_A^-\mathbf{X}^{-1}-\mu_m\mathbf{I}\delta_x^2\right)\right]\mathbf{H}^{-1} \times\left[\mathbf{H}+\Delta\tau\left(\delta_y^-\mathbf{Y}\mathbf{\Lambda}_B^+\mathbf{Y}^{-1}+\delta_y^+\mathbf{Y}\mathbf{\Lambda}_B^-\mathbf{Y}^{-1}-\mu_m\mathbf{I}\delta_y^2\right)\right]\Delta\mathbf{Q}^m=\mathbf{R}^m. \tag{5.7}$$

The system (5.7) can be solved with the well-known ADI scheme. Since the factor in each direction can be diagonalized, we only need to solve a system of scalar tri-diagonal equations like

$$a_j\Delta U_{j-1}+b_j\Delta U_j+c_j\Delta U_{j+1}=r_j,\quad j=1,\cdots,\text{jmax}-1$$

with periodic boundary condition $\Delta U_1=\Delta U_{\text{jmax}}$ for all cases in this work. In order to keep numerical stability, the split eigenvalues in LHS of Eq. (5.7) are constructed as

$$\mathbf{\Lambda}^{\pm}=\frac{1}{2}(\mathbf{\Lambda}\pm\kappa|\mathbf{\Lambda}|),$$

where $\kappa$ is a constant that is greater than or equal to unity to ensure the split eigenvalue is strictly positive or negative. $\kappa=1$ is used throughout this work.

## 6. Numerical examples

In this section, the numerical method developed in previous sections is tested on several 2D problems of incompressible two-fluid mixture. In all computations, we have used following fixed physical parameters:

$$\eta=0.02,\quad \lambda=0.1,\quad \mu=0.1,\quad \text{and}\quad \gamma=0.1$$

and the computational grid is $321\times321$ uniform grid points for a square solution domain $[0,2\pi]\times[0,2\pi]$. Time step $\Delta t$ is set to 0.002 so as to compare our results with the reference solutions [4,14,16], and CFL number for pseudo-time is set to 5. The maximum number of sub-iteration is set to 100 and the value of $\beta$ is fixed to 10. The initial velocity and pressure are all zero, while the initial condition for $\phi$ is specified in each example. We remark that the mesh size $2\pi/320=0.0196$ is comparable to the interfacial width $\eta$, implying that the diffusive layer is under-resolved.

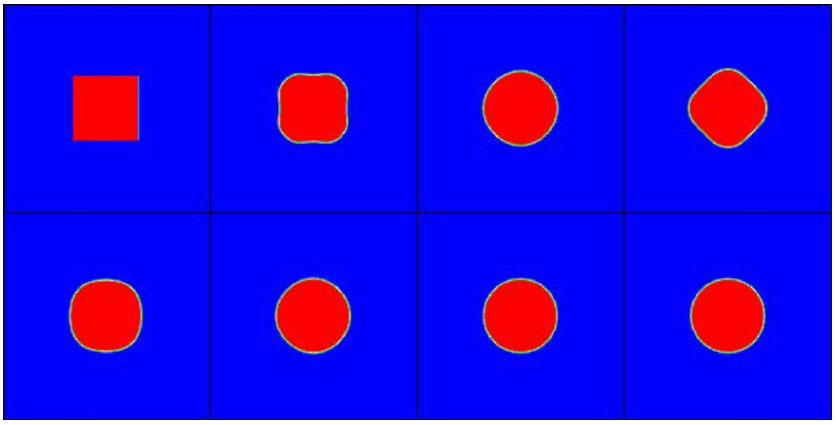

**Fig. 1.** Evolution of phase contours of an initially rectangle bubble with Lagrange multiplier at $t=0$, 0.1, 0.2, 0.4, 0.8, 1.2, 1.6, 2.0.

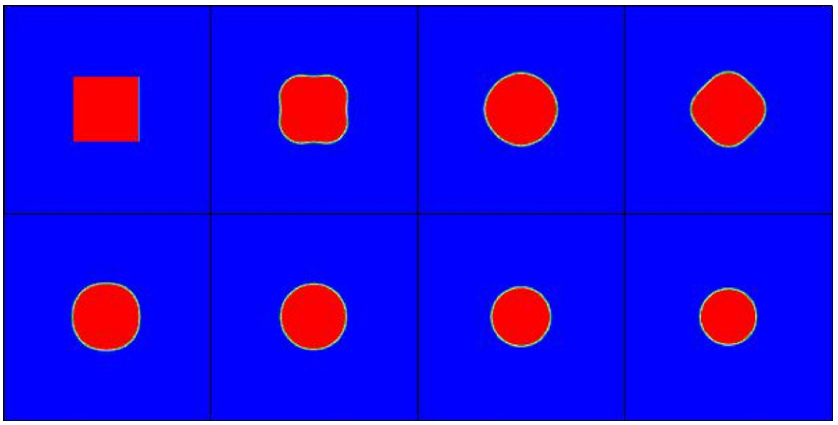

**Fig. 2.** Evolution of phase contours of an initially rectangle bubble without Lagrange multiplier at $t=0$, 0.1, 0.2, 0.4, 0.8, 1.2, 1.6, 2.0.

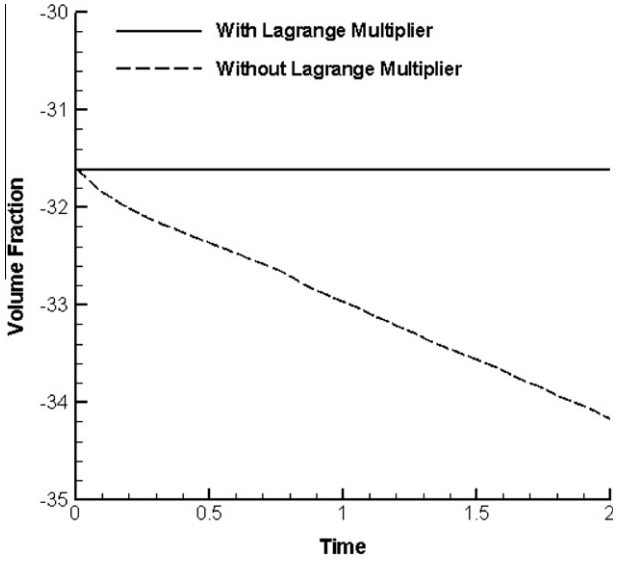


**Fig. 3.** Overall volume fraction versus time to show mass conservation.

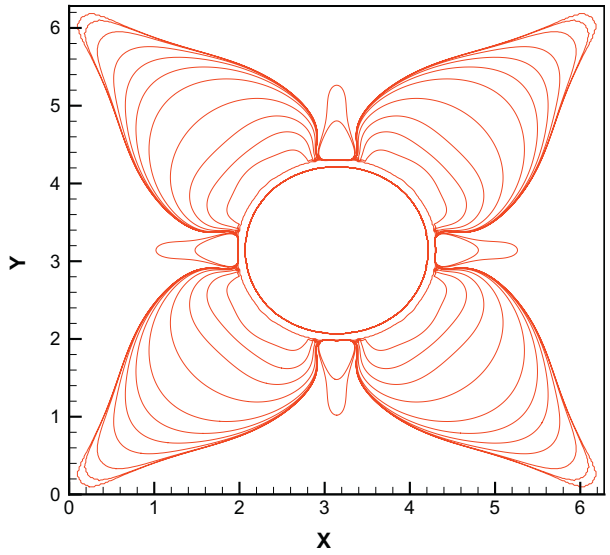


**Fig. 5.** Pressure contours of an initially rectangle bubble at time $t = 2.0$.

### 6.1. Example 1 (surface tension effects)

In this example, we give the evolution of a square to a circle to show the surface tension effects of the test problem. Initially a rectangular bubble is centered at $[\pi,\pi]$ with the side length of 2, and $\phi$ is taken 1 inside the bubble and $-1$ otherwise. As the time goes, the rectangular bubble deforms into a circular bubble due to the surface tension effect as shown in Fig. 1. However, if we remove the Lagrange multiplier from the phase field equation, the rectangular bubble will start shrinking as shown in Fig. 2. We observe that the volume of the bubble is preserved quite well with Lagrange multiplier, while it decreases gradually if no Lagrange multiplier is used, as shown in Fig. 3. The distribution of phase $\phi$ along $y = \pi$ is shown in Fig. 4 for $t = 2.0$ which is comparable with the final steady state circle of radius $\sqrt{4/\pi}$ centered at $(\pi,\pi)$. The pressure contours for this case are shown in Fig. 5 at $t = 2.0$. These results suggest the evolution processes of the bubble are in fair agreement with the reference solution [4].

Finally, to show the time accuracy of the scheme, the residual of the equations is shown in Fig. 6. We see it reduces by two orders of magnitude in 100 sub-iterations as evidenced from the enlarged subset for physical time $t = 1.5$. The CPU time up to $t = 2.0$ is about 10 h on a single core of Intel Xeon 5570.

### 6.2. Example 2 (cross to circle)

In this example, initially a cross is centered at $[\pi,\pi]$ with the side length of 4, $\phi$ is taken 1 inside the cross and $-1$ otherwise as shown in Fig. 7 ($t = 0.0$). The cross initially with sharp corners is finally deformed into a circle. This evolution of the phase exhibits the fact that the Allen–Cahn equation handles the sharp corners and minimizes the measure of the interface [32]. The final state of the deformation is a steady state circle with a minimum size of the interface. The results shown in Fig. 7 are well comparable to those obtained by using the finite element method [32].

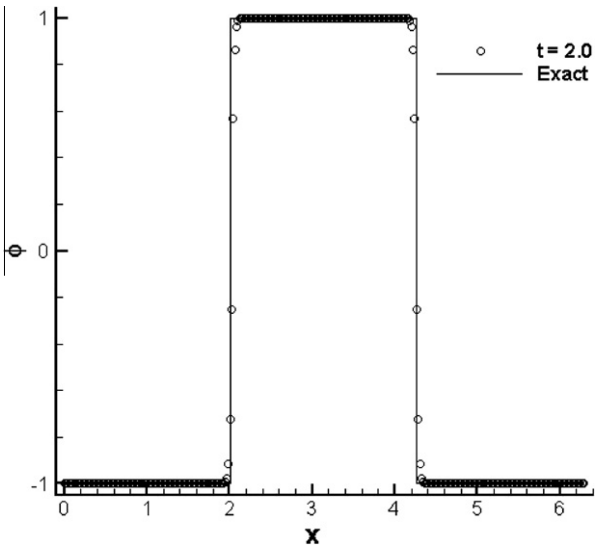


**Fig. 4.** Comparison of computed profile of $\phi$ along $y = \pi$ at $t = 2.0$ with the exact circle of radius $\sqrt{4/\pi}$ centered at $(\pi,\pi)$.

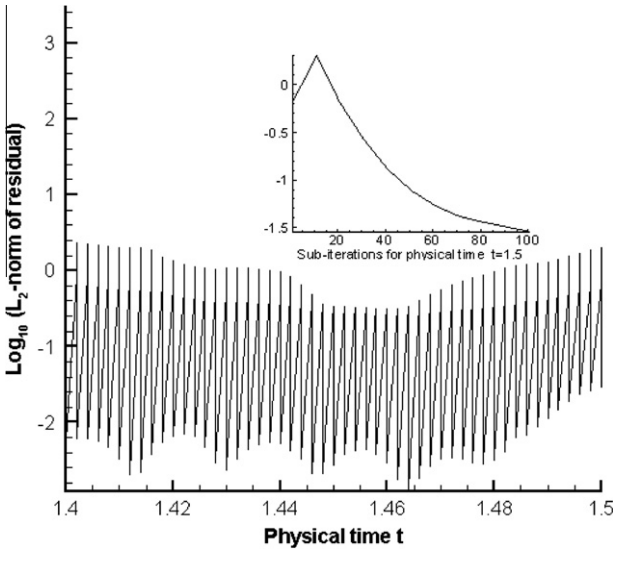


**Fig. 6.** Convergence history from physical time at $t = 1.4$ to $t = 1.5$ with 100 sub-iteration in psuedo-time. The enlarged subfigure shows the convergence after 100 sub-iteration at physical time $t = 1.5$.

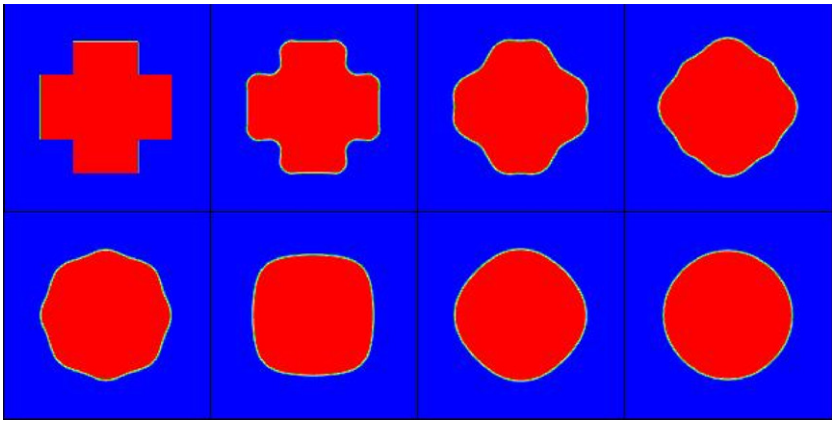

**Fig. 7.** Evolution of phase contours from a cross to a circle at $t = 0, 0.04, 0.12, 0.2, 0.4, 0.8, 1.6, 2.0$.

### 6.3. Example 3 (coalescence of two kissing bubbles)

In this example, the coalescence of two kissing bubbles is studied. Initially, two unit circular bubbles are centered at $[\pi - 1, \pi]$ and $[\pi + 1, \pi]$ respectively, As the time evolves, first the two bubbles coalesce into a big elliptical bubble, which then transfigures and deforms into a steady state circular bubble as shown in Fig. 8. This is the combination of the surface tension effect and the elastic effect from the phase equation [4].

### 6.4. Example 4 (coalescence of three kissing bubbles)

This example is to further study coalescence of three equal bubbles which are initially kissing each other. Their radii are all equal to $\pi/4$, and $\phi$ is taken as 1 inside these bubbles and $-1$ otherwise. Fig. 9 presents contours of the phase field $\phi$ at several different time instants. As the time evolves, first the three bubbles coalesce into one big bubble due to the surface tension, then that big bubble deforms into an inverted triangle bubble at $t = 0.2$. This deforma-

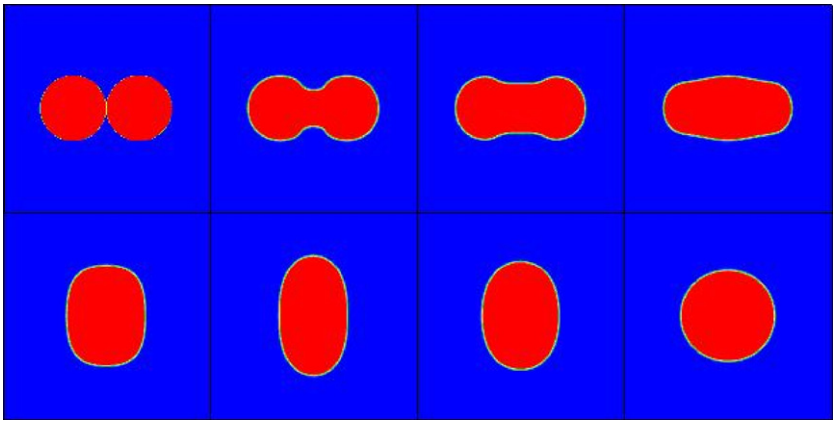

**Fig. 8.** Contours of phase $\phi$ for initially two kissing bubbles at $t = 0, 0.1, 0.2, 0.4, 1.2, 2.0\ 2.4, 2.8$.

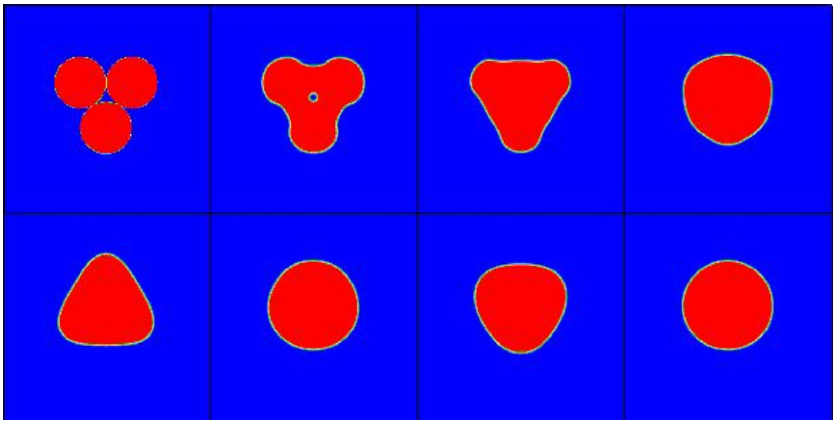

**Fig. 9.** Contours of phase $\phi$ for initially three kissing bubbles at $t = 0, 0.1, 0.2, 0.4, 0.8, 1.2, 1.6, 2.0$.

tion procedure continues alternately until the bubble reaches a steady circular bubble. The present results are in good agreement with those obtained by using the moving mesh method [15].

## 7. Conclusions

We have proposed a new numerical method for the phase field model for simulating incompressible two-phase flows based on the artificial compressibility approach. A modified Allen–Cahn type of phase field equation for the mixture of two incompressible fluids is coupled with the Navier–Stokes equations in a fairly simple way. The numerical results demonstrate that high-order high-resolution WENO schemes can be used in conjunction with the artificial compressibility method, and it can correctly capture a thin diffusive layer even if meshes are not fine enough to resolve that layer. The modified Allen–Cahn equation is shown capable of preserving volume fraction. The present results are comparable to other calculated ones. Future work may include implicit treatment of capillary effects and nonlinear terms to relax physical time step, modeling of different densities and viscosities, and extension to 3D problems.

## Acknowledgments

This work was carried out while A. Shah was visiting LSEC. The visit was supported jointly by LSEC and HEC Pakistan under Pakistan Organization of Collaborative Research (POCR). The work of L. Yuan was supported by Natural Science Foundation of China (10729101, 10972230) and state key program for developing basic sciences (2005CB321703, 2010CB731505).

## References

[1] Young T. An essay on the cohesion of fluids. Philos Trans Roy Soc Lond 1805;95:65–87.
[2] Rayleigh Lord. On the theory of surface forces. Philos Mag 1892;33:209–20.
[3] van der Waals JD. The thermodynamic theory of capillarity under the hypothesis of a continuous variation of density (English translation). J Stat Phys 1979;20:197–244.
[4] Liu C, Shen J. A phase field model for the mixture of two incompressible fluids and its approximation by a Fourier-spectral method. Physica D 2003;179:211–28.
[5] Desjonqueres MC, Spanjaard D. Concepts in surface physics. Springer series in surface sciences, vol. 30. Berlin: Springer; 1993.
[6] Lowengrub J, Truskinovsky L. Quasi-incompressible Cahn–Hilliard fluids and topological transitions. Roy Soc Lond Proc Ser A Math Phys Eng Sci 1998;454:2617–54.
[7] Anderson DM, McFadden GB, Wheeler AA. Diffuse-interface methods in fluid mechanics. Appl Math Lett 1998;30(4):139–65.
[8] Feng JJ, Liu C, Shen J, Yue P. An energetic variational formulation with phase field methods for interfacial dynamics of complex fluids: advantages and challenges. In: Maria-Carme T, Eugene M, editors. Modeling of soft matter, the IMA volumes in mathematics and its applications, vol. 141. New York: Springer; 2005. p. 1–26.
[9] Yue P, Feng JJ, Liu C, Shen J. A diffuse-interface method for simulating two-phase flows of complex fluids. J Fluid Mech 2004;515(1):293–317.
[10] Yue P, Feng JJ, Liu C, Shen J. Diffuse-interface simulations of drop coalescence and retraction in viscoelastic fluids. J Non-Newton Fluid Mech 2005;129:163–76.
[11] Yue P, Feng JJ, Liu C, Shen J. Interfacial force and Marangoni flow on a nematic drop retracting in an isotropic fluid. J Colloid Interface Sci 2005;290:281–8.
[12] Yang XF, Feng JJ, Liu C, Shen J. Numerical simulations of jet pinching-off and drop formation using an energetic variational phase field method. J Comput Phys 2006;218:417–28.
[13] Liu C. Variational approach in two-phase flows of complex fluids: transport and induced elastic stress. In: Miranville A, editor. Mathematical models and methods in phase transitions. Nova Publications; 2005.
[14] Di YN, Li R, Tang T. A general moving mesh framework in 3D and its application for simulating the mixture of multi-phase flows. Commun Comput Phys 2008;3(3):582–602.
[15] Zhang ZR, Tang HZ. An adaptive phase field method for the mixture of two incompressible fluids. Comput Fluids 2007;36:1307–18.
[16] Tan ZJ, Lim KM, Khoo BC. An adaptive mesh redistribution method for the incompressible mixture flows using phase field model. J Comput Phys 2007;225:1137–1158,.
[17] Cahn JW, Allen SM. A microscopic theory of domain wall motion and its experimental verification in Fe–Al alloy domain growth kinetics. J Phys 1977;38:47–51.
[18] Cahn JW, Hilliard JE. Free energy of a non-uniform system. I. Interfacial energy. J Chem Phys 1958;28(2):258–67.
[19] Jacqmin D. Calculation of two-phase Navier–Stokes flows using phase field modeling. J Comput Phys 1999;155:96–127.
[20] Osher S, Sethian JA. Fronts propagation with curvature-dependent speed: algorithm based on Hamilton–Jacobi formulations. J Comput Phys 1988;79:12–49.
[21] Sethian JA. Level set methods and fast marching methods. Cambridge monographs on applied and computational mathematics, vol. 3. Cambridge: Cambridge University Press; 1999.
[22] Chorin AJ. A numerical method for solving incompressible viscous flow problems. J Comput Phys 1967;2:12–26.
[23] Sun Pengtao, Liu Chun, Xu Jinchao. Phase field model of thermo-induced Marangoni effects in the mixtures and its numerical simulations with mixed finite element method. Commun Comput Phys 2009;6:1095–117.
[24] Tan Z, Tang T, Zhang Z. A simple moving mesh method for one- and two-dimensional phase field equations. J Comput Appl Math 2006;190:252–69.
[25] Jiang GS, Shu CW. Efficient implementation of weighted ENO schemes. J Comput Phys 1996;126:202–28.
[26] Yang JY, Yang SC, Chen YN, Hsu CA. Implicit weighted ENO schemes for three-dimensional incompressible Navier–Stokes equations. J Comput Phys 1998;146:464–87.
[27] Rogers SE, Kwak D. An upwind differencing scheme for the time-accurate incompressible Navier–Stokes equations. AIAA J 1990;28(2):253–62.
[28] Shah A, Yuan L, Khan A. Upwind compact finite difference scheme for time-accurate solution of the incompressible Navier–Stokes equations. Appl Math Comput 2010;215(9):3201–13.
[29] Beam R, Warming RF. An implicit scheme for the compressible Navier–Stokes equations. AIAA J 1978;16:393–402.
[30] Pulliam T, Chaussee D. A diagonal form of an implicit approximate factorization algorithm. J Comput Phys 1981;39:347–63.
[31] Yuan L. Comparison of implicit multigrid schemes for three-dimensional incompressible flows. J Comput Phys 2002;177:134–55.
[32] Kay D, Welford R. A multigrid finite element solver for the Cahn–Hilliard equation. J Comput Phys 2006;212:288–304.